Front. Optoelectron. 2013, 6(3): 282–289
DOI 10.1007/s12200-013-0334-x

RESEARCH ARTICLE

# Strain effects on performance of electroabsorption optical modulators

**Kambiz ABEDI (✉)**

Department of Electrical Engineering, Faculty of Electrical and Computer Engineering, Shahid Beheshti University, Tehran 1983963113, Iran



**Abstract** This paper reports a detailed theoretical investigation of strain effects on the performance of electroabsorption optical modulators based on the asymmetric intra-step-barrier coupled double strained quantum wells (AICD-SQWs) active layer. For this purpose, the electroabsorption coefficient was calculated over a range of AICD-SQWs strain from compressive to tensile strain. Then, the extinction ratio (ER) and insertion loss parameters were evaluated from calculated electroabsorption coefficient for transverse electric (TE) input light polarization. The results of the simulation suggest that the tensile strain from 0.05% to 0.2% strain in the wide quantum well has a significant impact on the ER and insertion loss as compared with compressive strain, whereas the compressive strain of the narrow quantum well from −0.5% to −0.7% strain has a more pronounced impact on the improvement of the ER and insertion loss as compared with tensile strain.

**Keywords** asymmetric intra-step-barrier coupled double strained quantum wells (AICD-SQWs), electroabsorption modulators, strain, insertion loss

## 1 Introduction

Electroabsorption optical modulators (EAMs) based on the quantum confined Stark effect (QCSE) of a multiple quantum wells (MQW) structure are suitable components in high-speed long-distance fiber-optic links and transmissions for both telecom and data-com applications. Their advantages include small size, low chirp, low driving voltage, high extinction ratio (ER), high modulation efficiency, wide modulation bandwidth. In addition, due to matching of material systems, EAMs can be easily integrated with other optical components, such as semiconductor lasers, semiconductor optical amplifiers, and attenuators in contrast to optical modulators made in for instance $LiNbO_3$ [1,2]. Furthermore, an EAM has a drawback of large insertion loss resulted from a residual absorption and a mode mismatch to a single mode fiber in comparison with $LiNbO_3$ optical modulator [3].

For the purpose of having high radio frequency (RF) link gain, large spurious free dynamic range (SFDR), small noise figure and large bandwidth in analog fiber-optic links, small insertion loss, large modulation efficiency and high optical power handling capacity are required for optical modulator [4,5].

To investigate EAM performance, many characteristics must be simultaneously investigated. The insertion loss of an EAM should be as low as possible to avoid optical power attenuation. The ER should be large, to keep the bit-error-rate (BER) low, and to reduce power penalty. For many telecommunications applications, the chirp should be low, or preferably negative, to compensate for the dispersive properties of the optical fiber [6,7]. However, most EAMs based on the QCSE impose a large insertion loss ranging from 6 to 12 dB even at zero bias voltage [8] and produce positive chirp parameter. Consequently, the reduction of insertion loss and chirp parameter without the outlay of a high ER is an important issue for EAMs with both asymmetric and strained-layer quantum wells.

Recently, the asymmetric intra-step-barrier coupled double strained quantum wells (AICD-SQWs) structure has been demonstrated to suppress the red shift of the QCSE to a higher electric field and to reduce the oscillator strength at zero fields [9–19]. With coupled double strained quantum well (QW), asymmetric quantum wells can deeply separate electron and heavy hole wave functions at zero electric field, thereby decreasing the insertion loss when it is incorporated into the EAM. Due to the increased operation electric field and decreased the spatial overlap integral between the electron and the hole envelope wave functions, the EAM based on AICD-SQWs active layer

Received April 22, 2013; accepted June 17, 2013

E-mail: K_Abedi@sbu.ac.ir

can have a higher saturation optical power and very low insertion loss than the conventional QW and intra-step quantum well (IQW) EAM and therefore provide advantages such as enhanced RF link gain. In addition to aforementiond merits, the AICD-SQWs structure has large Stark shift, large change in absorption, high ER, zero chirp parameter and higher figures of merit as compared with IQW structure at 1.55 μm. This paper intends to investigate the effect of strain in the well layers of AICD-SQWs structure on the ER and insertion loss parameters over a wide range of strain from compressive to tensile.

Considering the AICD-SQWs structure with $In_{(1-x-y)}Ga_xAl_yAs$ wells and with $In_{0.52}Al_{0.48}As$ barriers, a numerical simulation is developed, to analyze the strain effect of wells on the ER and insertion loss parameters in EAM. For this purpose, first, the electron and hole subband energy levels and their envelope wave functions are calculated using transfer matrix method (TMM) considering finite barrier, strain effect and applied electric field [9–13]. Then, the optical matrix elements of the structures for transverse electric (TE) and transverse magnetic (TM) polarization are calculated. The exciton equation in momentum space is solved numerically using the Gaussian quadrature method (GQM) [9,10] to obtain the exciton binding energy and oscillator strength. The electroabsorption coefficient is calculated for different applied electric field for TE input light polarization. Finally, the ER and insertion loss parameters are calculated for different strains.

## 2 AICD-SQWs structure

A schematic illustration of the AICD-SQWs structure is shown in Fig. 1 [9–15]. The figure also illustrates the direction of the applied electric field ($F$). The undoped AICD-SQWs structure has $In_{0.52}Al_{0.48}As$ barriers, which are lattice matched to the InP substrate, as well as one lattice-matched $In_{0.53}Ga_{0.33}Al_{0.14}As$ intra-step-barrier. The $In_{0.525}Ga_{0.475}As$ wide well is under 0.05% of tensile strain (TS), and the $In_{0.608}Ga_{0.392}As$ narrow well is under 0.52% of compressive strain (CS). The thickness of each of the two external barriers is 10 nm, while the thickness of the middle barrier is 1.5 nm. The thicknesses of the wide well, the narrow well and the intra-step-barrier are 6.8, 3.5 and 4 nm, respectively.

The middle barrier layer and strain amount of wells cause the electron and heavy hole wave functions are distributed dominantly in the wide and narrow wells, respectively. As a result, the insertion loss significantly decreases at zero electric field.

The optical modulator length and optical confinement factor are taken to be 200 μm and 0.15, respectively. It should be noted that the well thicknesses of original structure are theoretically set to have the exciton peak at ~1.51 μm for zero electric field [9].

| | |
|---|---|
| $In_{0.52}Al_{0.48}As$ | 10 nm |
| $In_{0.53}Ga_{0.33}Al_{0.14}As$ | 4 nm |
| $In_{0.525}Ga_{0.475}As$ | 6.8 nm |
| $In_{0.52}Al_{0.48}As$ | 1.5 nm |
| $In_{0.608}Ga_{0.392}As$ | 3.5 nm |
| $In_{0.52}Al_{0.48}As$ | 10 nm |

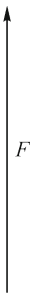


**Fig. 1** Schematic of layers for the AICD-SQWs structure, and direction of applied electric field ($F$) is indicated as well

## 3 Theory of numerical simulation

The field-dependent absorption spectrum of the AICD-SQWs structure as shown in Fig. 1 is calculated by the following procedure. The subbands and the envelope functions of electrons, heavy holes, and light holes under an applied electric field ($F$) are calculated using TMM. Conduction and valence bands are assumed parabolic in our calculations. The conduction band Hamiltonian under an applied electric field ($F$) is given by [9]

$$H_C = \frac{\hbar^2}{2m_e^*}(k_x^2 + k_y^2 + k_z^2) + C_1(\varepsilon_{xx} + \varepsilon_{yy} + \varepsilon_{zz}) + V_0(z) - eFz, \quad (1)$$

$$H_e(z) = -\frac{\hbar^2}{2}\frac{\partial}{\partial z}\left(\frac{1}{m_e^*(z)}\frac{\partial}{\partial z}\right) + V_e(z) - eFz, \quad (2)$$

$$E = E_t + E_n^e = \frac{\hbar^2(k_x^2 + k_y^2)}{2m_e^*} + E_n^e, \quad (3)$$

where, $z$ is the growth direction, $\hbar$ is the reduced Planck constant, $m_e^*$ is the electron effective mass, $C_1$ is the deformation potential for the conduction band, $V_0(z)$ is the height of quantum well, $V_e(z)$ is the quantum well confining potential in growth direction for the electron, and $E_n^e$ is the eigenvalue of Schrödinger equation. The effects of strain are calculated in the following way. The strain in the plane of the epitaxial growth is

$$\varepsilon = \varepsilon_{xx} = \varepsilon_{yy} = \frac{a_0 - a}{a_0}, \quad (4)$$

where $a$ is the lattice constant of the quaternary epitaxial layer and $a_0$ is the lattice constant of the substrate, InP. The strain in the perpendicular direction can be expressed as

$$\varepsilon_{zz} = -\frac{2C_{12}}{C_{11}}\varepsilon, \quad \varepsilon_{xy} = \varepsilon_{xz} = \varepsilon_{zy} = 0, \quad (5)$$

where $C_{11}$ and $C_{12}$ are the elastic stiffness constants. The strain shift in the conduction band is determined by [9]

$$\delta E_{\rm c}(x,y) = a_{\rm c}(\varepsilon_{xx}+\varepsilon_{yy}+\varepsilon_{zz}) = 2a_{\rm c}\left(1-\frac{C_{12}}{C_{11}}\right)\varepsilon, \quad (6)$$

and the strain shift for light an heavy holes in the valence bands are determined by

$$\delta E_{hh}(x,y) = -P_\varepsilon - Q_\varepsilon,\ \delta E_{lh}(x,y) = -P_\varepsilon + Q_\varepsilon, \quad (7)$$

where

$$P_\varepsilon = -a_{\rm v}(\varepsilon_{xx}+\varepsilon_{yy}+\varepsilon_{zz}) = -2a_{\rm v}\left(1-\frac{C_{12}}{C_{11}}\right)\varepsilon,$$

$$Q_\varepsilon = -\frac{b}{2}(\varepsilon_{xx}+\varepsilon_{yy}-2\varepsilon_{zz}) = -2b\left(1+2\frac{C_{12}}{C_{11}}\right)\varepsilon. \quad (8)$$

Thus, for the conduction and the valence subbands, the strained quantum well potentials are determined by

$$V_{\rm e}(z) = \begin{cases} \delta E_{\rm c} = 2a_{\rm c}\left[1-\dfrac{C_{12}}{C_{11}}\right]\varepsilon, & |z| \leqslant L_z, \\ V_0 = \Delta E_{\rm c} = Q_{\rm e}\Delta E_{\rm g}, & |z| > L_z, \end{cases}$$

$$V_{\rm h}(z) = \begin{cases} \delta E_{hh(lh)} = 2a_{\rm v}\left[1-\dfrac{C_{12}}{C_{11}}\right]\varepsilon \pm 2b\left(1+2\dfrac{C_{12}}{C_{11}}\right)\varepsilon, & |z| \leqslant L_z, \\ V_0 = \Delta E_{hh(lh)} = Q_{hh(lh)}\Delta E_{\rm g}, & |z| > L_z, \end{cases} \quad (9)$$

where $a_{\rm c}$ and $a_{\rm v}$ are the conduction band and valence band hydrostatic deformation potentials, $b$ is the valence band shear deformation potential, $C_{11}$ and $C_{12}$ are the elastic stiffness constants, $\varepsilon$ is the strain in the plane of the epitaxial growth, $\Delta E_{\rm g}$ is the difference in the bulk bandgap between well and barrier, $L_z$ is the effective thickness of the AICD-SQW, and $Q_{\rm e}$, $Q_{hh}$, and $Q_{lh}$ are band offsets using Harrison's model [9]. To obtain most parameters for the $In_{(1-x-y)}Ga_xAl_yAs$ material systems, a linear interpolation between the parameters of the relevant binary semiconductors is used.

### 3.1 Transfer matrix method

To analyze the quantization effect in quantum structure, we can solve the Schrödinger equation by using transfer matrix method. The time independent Schrödinger equation with an electric filed is given as follows

$$-\frac{\hbar^2}{2}\frac{\partial}{\partial z}\left(\frac{1}{m_{\rm e}^*(z)}\frac{\partial\psi(z)}{\partial z}\right) + \left(V_{\rm e}(z)-eFz\right)\psi(z) = E\psi(z), \quad (10)$$

where, $m_{\rm e}^*(z)$ is the effective mass, $\hbar$ is the Planck's constant, $e$ is the electron charge, $E$ is the eigen energy. $V_{\rm e}(z)$ is the quantum well confining potential in growth direction for the electron, $F$ is the applied electric field. For applying the transfer matrix scheme, we divide the structure into segments, which can vary in length. Potential and effective mass discontinuities can be treated exactly in transfer matrix approaches by applying corresponding matching conditions. For the piecewise constant potential approach, the potential and effective mass in each segment $j$ are approximated by constant values, e.g.,

$$V_{{\rm e}j} = V_{\rm e}(z_j),\ m_{{\rm e}j}^* = m_{\rm e}^*(z_j),$$

for

$$z_j \leqslant z < z_j + \Delta_j = z_{j+1},$$

and a jump

$$V_{{\rm e}j} \longrightarrow V_{{\rm e}(j+1)},\ m_{{\rm e}j}^* \longrightarrow m_{{\rm e}(j+1)}^*$$

at the end of the segment. The solution of Eq. (10) is for $z_j \leqslant z < z_{j+1}$ then given by [20]

$$\psi(z) = A_j\exp[{\rm i}k_j(z-z_j)] + B_j\exp[-{\rm i}k_j(z-z_j)], \quad (11)$$

where

$$k_j = \sqrt{2m_{{\rm e}j}^*(E-V_{{\rm e}j})}\big/\hbar$$

is the wavenumber. The matching conditions for the wavefunction at the potential step read

$$\begin{aligned} \psi(z_0+) &= \psi(z_0-), \\ [\partial_z\psi(z_0+)]/m_{\rm e}^*(z_0+) &= [\partial_z\psi(z_0-)]/m_{\rm e}^*(z_0-), \end{aligned} \quad (12)$$

where $z_0+$ and $z_0-$ denote the positions directly to the right and left of the step, here located at $z_0 = z_{j+1}$. The amplitudes $A_{j+1}$ and $B_{j+1}$ are related to $A_j$ and $B_j$ by

$$\begin{pmatrix} A_{j+1} \\ B_{j+1} \end{pmatrix} = \boldsymbol{T}_{j,j+1}\begin{pmatrix} A_j \\ B_j \end{pmatrix}, \quad (13)$$

with the transfer matrix

$$\boldsymbol{T}_{j,j+1} = \begin{pmatrix} \dfrac{\beta_{j+1}+\beta_j}{2\beta_{j+1}}{\rm e}^{{\rm i}k_j\Delta_j} & \dfrac{\beta_{j+1}-\beta_j}{2\beta_{j+1}}{\rm e}^{-{\rm i}k_j\Delta_j} \\ \dfrac{\beta_{j+1}-\beta_j}{2\beta_{j+1}}{\rm e}^{{\rm i}k_j\Delta_j} & \dfrac{\beta_{j+1}+\beta_j}{2\beta_{j+1}}{\rm e}^{-{\rm i}k_j\Delta_j} \end{pmatrix} \quad (14)$$

with $\beta_j = k_j/m^*_{ej}$, derived from Eq. (12). The relation between the amplitudes at the left and right boundaries of the structure, $A_0$, $B_0$ and $A_N$, $B_N$, can be obtained from

$$\begin{pmatrix} A_N \\ B_N \end{pmatrix} = \boldsymbol{T}_{N-1,N}\boldsymbol{T}_{N-2,N-1}\ldots\boldsymbol{T}_{0,1}\begin{pmatrix} A_0 \\ B_0 \end{pmatrix} = \begin{pmatrix} T_{11} & T_{12} \\ T_{21} & T_{22} \end{pmatrix}\begin{pmatrix} A_0 \\ B_0 \end{pmatrix}, \quad (15)$$

where $N$ is the total number of segments. For bound states, this equation must be complemented by suitable boundary conditions. One possibility is to enforce decaying solutions at the boundaries, $A_0 = B_N = 0$, corresponding to $T_{22} = 0$ in Eq. (14), which is satisfied only for specific energies $E$, the eigenenergies of the bound states.

### 3.2 Electroabsorption spectrum

The electroabsorption spectrum $\alpha$ ($h\nu$) is related to the imaginary part of the dielectric constant, $\varepsilon_{\rm i}(h\nu)$, given as [9]

$$\alpha(h\nu) = \frac{2\pi}{\lambda_0 n_{\rm r}}\varepsilon_{\rm i}(h\nu) = \frac{\omega}{cn_{\rm r}}\varepsilon_{\rm i}(h\nu), \quad (16)$$

where $\lambda_0$, $c$, and $n_{\rm r}$ are the free-space wavelength of incident light, the speed of light in vacuum, and the refractive index, respectively. $\alpha(h\nu)$ in Eq. (16) can be defined as

$$\alpha(h\nu) = \alpha(h\nu)^{\rm band} + \alpha(h\nu)^{\rm exciton}. \quad (17)$$

The first term is due to the band-to-band transitions and the second term is due to the excitonic transitions. The electroabsorption coefficient of the band-to-band transitions between $n$th subband electrons and $m$th subband holes is written as

$$\alpha(h\nu)^{\rm band} = \frac{e^2}{\varepsilon_0 m_0^2 cn_{\rm r}\omega L_z}\cdot\frac{\mu}{\hbar^2}\int M_{nm}^2(E) \times L(h\nu - E - E_{\rm g} - E_n^{\rm e} - E_m^{\rm h})\mathrm{d}E, \quad (18)$$

where $\varepsilon_0$ is the dielectric constant, $m_0$ the free-electron mass, $n_{\rm r}$ the refractive index, $L_z$ the effective thickness of the AICD-SQW, $E_{\rm g}$ the energy gap, $\mu$ the reduced mass for the motion in the $x$-$y$ plane, and $L(y)$ the line shape function for each transition, respectively.

Here, we assume that $L(y)$, Lorentzian line shape function with zero-field FWHM, is 10 meV. The quantity $M_{nm}(E)$ is$(\xi\cdot P_{\rm cv})|I_{nm}|$, where $\xi$ is the polarization vector, $P_{\rm cv}$ is momentum matrix element between the conduction band and valence band Bloch functions, and $|I_{nm}|$ is the overlap integral between the conduction and valence subbands wave functions. For calculation of the contribution of exciton transitions between $n$th subband electron and $m$th subband hole, the exciton equation in momentum space (Eq. (20)) is solved numerically using the Gaussian quadrature method for 1$s$ exciton state [9]:

$$\left(E_n^{\rm e}(k) + E_m^{\rm h}(k)\right)\phi_{nm}^X(k) + \sum_{n'm'}\int\frac{\mathrm{d}^2k'}{(2\pi)^2}V(k,k')\phi_{nm}^X(k') = E_X\phi_{nm}^X(k), \quad (19)$$

$E_X$ is the transition energy for 1$s$ exciton state and $V(k, k')$ corresponding to coulomb interaction, defined as

$$V(k,k') = -\frac{e^2}{4\pi\varepsilon}\int\mathrm{d}z_{\rm e}\int\mathrm{d}z_{\rm h}\int\frac{\mathrm{d}\theta}{q}\exp(-q|z_{\rm e}-z_{\rm h}|) \times f_n(z_{\rm e})f_{n'}(z_{\rm e})g_m(k,z_{\rm h})g_{m'}(k',z_{\rm h}), \quad (20)$$

where $q$ is $(k^2 + k'^2 - 2kk'\cos\theta)^{1/2}$ and $\phi_{nm}^X(k)$ , the exciton envelop wave function in momentum space. $E_n^{\rm e}(k)$ , $E_m^{\rm h}(k)$, $f_n(z_{\rm e})$ and $g_m(k,z_{\rm h})$ are the electron and hole energy levels and wave functions, respectively, calculated by TMM solution for the AICD-SQWs structure Hamiltonian under an applied electric field ($F$).

$$H_{\rm e} = E_{\rm c}(-{\rm i}\nabla) + V_{\rm e}(z) - eFz,$$

$$H_{\rm h} = H^{\rm LK} + V_h(z) + eFz, \quad (21)$$

where $E_{\rm c}(-{\rm i}\nabla)$ is electron kinetic energy operator, and $H^{\rm LK}$ is 4 × 4 Luttinger-Kohn tensor. The exciton oscillator strength for this state is defined as [9]

$$f_X = \frac{2}{m_0 E_X}\left|\int\frac{\mathrm{d}^2k}{(2\pi)^2}\phi_{nm}^X(k)M_{nm}(k)\right|^2, \quad (22)$$

and exciton binding energy is given by

$$E_B = E_X - E_n^{\rm e} - E_m^{\rm h} - E_{\rm g}. \quad (23)$$

So, the electroabsorption coefficient of an exciton transitions is written as

$$\alpha(h\nu)^{\rm exciton} = \frac{\pi e^2\hbar}{n_{\rm r}\varepsilon_0 m_0 cL_z}\sum_X f_X L(h\nu - E_X). \quad (24)$$

### 3.3 Extinction ratio parameter

The ER parameter is determined by the change in absorption coefficient between the on and off states ($\Delta\alpha$) for a given overlap of the optical mode with the AICD-SQWs structure ($\Gamma$) and optical modulator length ($L$) [21 – 24], defined as

$$ER[\mathrm{dB}]$$

$$= 10\log\frac{P_{\mathrm{out}}(L,V)}{P_{\mathrm{out}}(L,V=0)}$$

$$= 4.343\cdot\Gamma\cdot[\alpha(V=0)-\alpha(V)]\cdot L = 4.343\cdot\Gamma\cdot\Delta\alpha\cdot L, \quad (25)$$

where $P_{\mathrm{out}}$ is the level of output power, written as

$$P_{\mathrm{out}}(L,V) = P_0\exp\Big(-\Gamma\alpha(V)L\Big),$$

where $P_0$ is the initial light power, $\Gamma$ is the optical confinement factor at the electroabsorption layer, and $L$ is the modulator length.

### 3.4 Insertion loss parameter

Insertion loss consists of three parts: reflection loss at the facets, coupling loss from/to the optical fiber, and the optical propagation loss. The propagation loss is the main contributor to the insertion loss. It mainly depends on the waveguide scattering loss, free carrier absorption loss and the EA material residual absorption loss [21–24]. The insertion loss due to residual absorption, $IL$ (unit: dB), is given by

$$IL = 4.343\cdot\Gamma\cdot\alpha_0\cdot L, \quad (26)$$

where $\alpha_0$ is the static electroabsorption coefficient in the ON state. The insertion loss increases very quickly as the waveguide length increases. Values of $IL$ up to 2.5 dB are desirable for EA optical modulators.

## 4 Numerical simulation results and discussion

Now we investigate the effect of strain in the wide well layer from compressive to tensile with a fixed right well strain of −0.52% (CS) on the ER and insertion loss parameters in EAMs with AICD-SQWs for different values of applied electric field ($F$) between 0 and 120 kV/cm at $\lambda$ = 1.55 μm. For this purpose, the electroabsorption coefficient has been calculated. Figure 2 illustrates the strain dependence of absorption coefficient for TE input light polarization.

In Fig. 2, an increase of the electric field decreases the peak value of absorption coefficient and shifts the peak position toward tensile strain side. With applying tensile strain to the wide well, the oscillator strength, which is proportional to the square of the spatial overlap integral between the electron and the hole envelope wave functions, is increased in higher electrical fields. Therefore, the tensile strains of the wide well layer enhance the absorption in higher electrical fields.

The ER as function of the wide well layer strain at $\lambda$ = 1.55 μm was obtained from the calculated absorption curves for different values of the applied electric field by subtracting its values for different electrical fields from that for the lowest nonzero electrical field. Figure 3 shows the ER parameter of the AICD-SQWs in terms of wide well strain for applied electric fields of 20, 60, 100, and 120 kV/cm.

Large negative ER can be seen at around 0.2% CS due to the reduction in the oscillator strength for the lowest state subband excitons. Their positive peak value of ER parameter is summarized in Table 1.

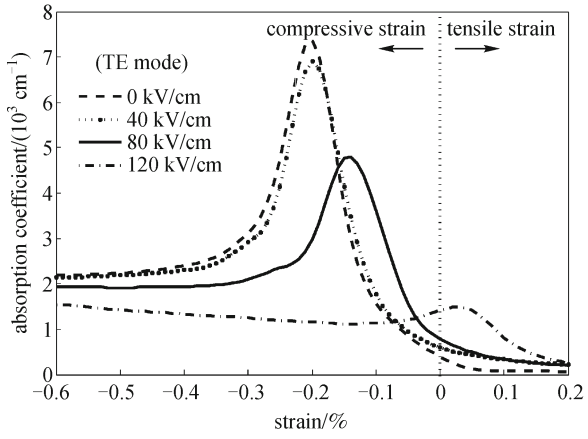


**Fig. 2** Absorption coefficient as function of the wide well layer strain at $\lambda$ = 1.55 μm

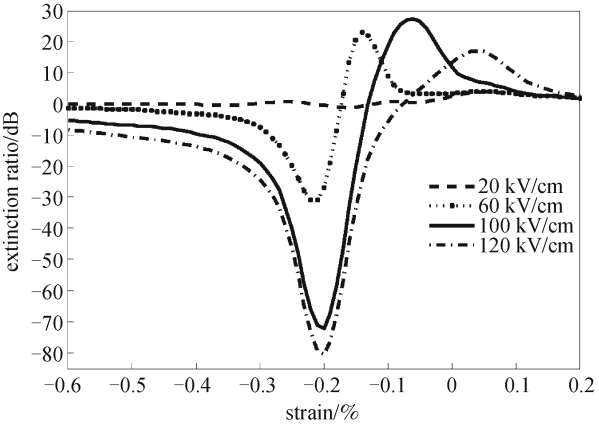


**Fig. 3** Calculated ER parameter as function of the wide well layer strain at $\lambda$ = 1.55 μm

**Table 1** Positive peak value of ER with various electric fields

| electric field/(kV·cm$^{-1}$) | extinction ratio/dB | wide well strain/% |
|---|---|---|
| 20 | 3.82 | 0.06 |
| 60 | 23.16 | −0.14 |
| 100 | 27.45 | −0.06 |
| 120 | 17.04 | 0.04 |

From the table, we can see that the positive peak value of ER parameter moves toward tensile strain side when the electric field increases.

Figure 4 also shows the calculated insertion loss parameter as function of the wide well layer strain at $\lambda$ = 1.55 μm for TE polarization. The peak value of the insertion loss parameter occurs near −0.2% strain (CS) and increases dramatically to about 97 dB.

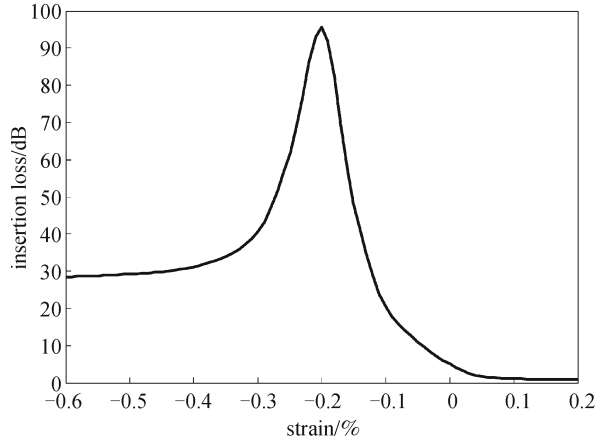


**Fig. 4** Calculated insertion loss parameter as function of the wide well layer strain at $\lambda$ = 1.55 μm

The insertion loss values will be high over compressive strain. As we can see from Fig. 4, the low insertion loss only can achieve by tensile strain of the wide well. Generally, tensile strain of the wide well provides significant advantages in producing large ER and low insertion loss as compared with compressive strain. Therefore, tensile strain of the wide well will be suitable for practical device operation.

The ER parameter versus insertion loss for various electric fields at $\lambda$ = 1.55 μm is shown in Fig. 5. As we mentioned above, insertion loss values of EAMs up to 2.5 dB are desirable.

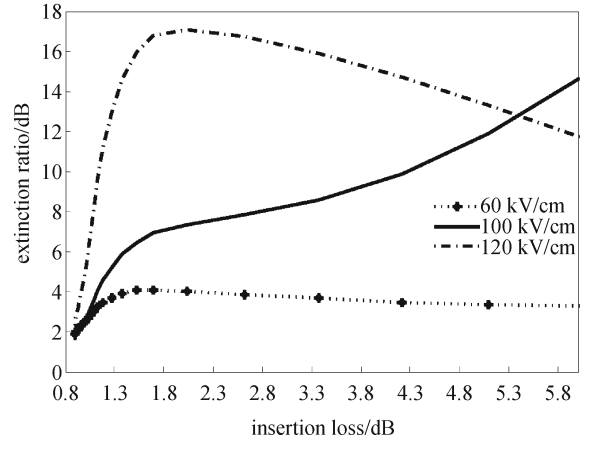


**Fig. 5** Calculated ER parameter versus insertion loss for various electric fields at $\lambda$ = 1.55 μm

Therefore, we consider the insertion loss below 2.5 dB that is corresponding to the wide well tensile strain from 0.05% to 0.2% strain. In this range, the maximum value of the ER parameter that is 17.1 dB, take places at insertion loss of 1.9 dB at electric field of 120 kV/cm.

Then, we investigate the effect of strain in the narrow well layer from compressive to tensile with the fixed left well strain of 0.05% (TS) on the ER and insertion loss parameters in EAMs with AICD-SQWs for different values of applied electric field ($F$) between 0 and 120 kV/cm at $\lambda$ = 1.55 μm.

Figure 6 shows the calculated ER parameter as function of the narrow well layer strain. This figure shows a considerable improvement in the ER when the compressive strain in the narrow well layer is increased from −0.5% to −0.7% strain.

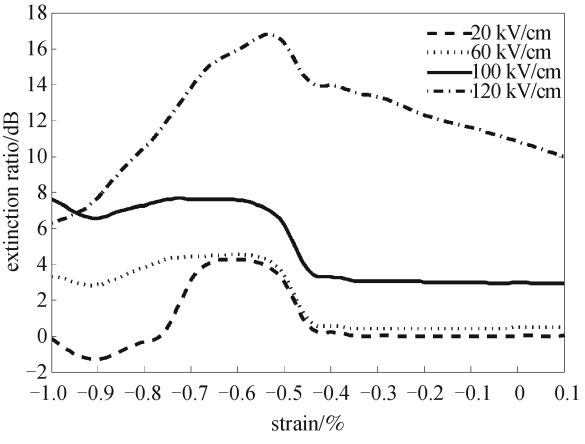


**Fig. 6** Calculated ER parameter as function of the narrow well layer strain at $\lambda$ = 1.55 μm

The calculated insertion loss parameter as function of the narrow well layer strain is shown in Fig. 7. As seen in this figure, the compressive strain of narrow well from −0.5% to −0.8% has significant effect on the insertion loss. The

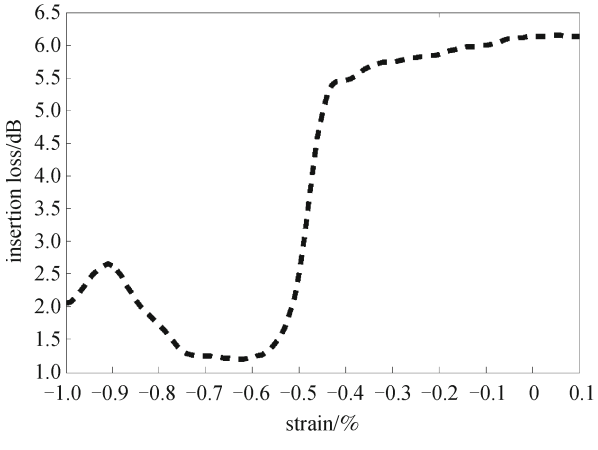


**Fig. 7** Calculated insertion loss parameter as function of the narrow well layer strain at $\lambda$ = 1.55 μm

value of insertion loss will be near 1.2 dB in this range of compressive strain.

## 5 Conclusions

In this paper, the strain effect of AICD-SQWs on the ER and insertion loss parameters in EAMs had been numerically simulated using the transfer matrix method. The electroabsorption coefficient was calculated over a wide range of AICD-SQWs strain from compressive to tensile. The ER and insertion loss parameters were evaluated from calculated electroabsorption coefficient for TE input light polarization. The results of the simulation suggest that the tensile strain from 0.05% to 0.2% strain in the wide quantum well has a significant impact on the ER and insertion loss as compared with compressive strain, whereas the compressive strain of the narrow quantum well from $-0.5\%$ to $-0.7\%$ strain has a more pronounced impact on the improvement of the ER and insertion loss as compared with tensile strain.

**Acknowledgements** The author would like to express his gratitude to Professor V. Ahmadi and Dr. E. Darabi for the useful discussions.

## References

1. Irmscher S, Lewen R, Eriksson U. InP-InGaAsP high-speed traveling-wave electroabsorption modulators with integrated termination resistors. IEEE Photonics Technology Letters, 2002, 14(7): 923–925
2. Kim J, Kang Y S, Chung YD, Choi K S. Development and RF characteristics of analog 60-GHz electroabsorption modulator module for RF/optic conversion. IEEE Transactions on Microwave Theory and Techniques, 2006, 54(2): 780–787
3. Kang Y S, Kim S B, Chung Y D, Kim J. Low insertion loss electroabsorption modulator based on dual waveguide sturcture with spot size converter. In: The 18th Annual Meeting of the IEEE Lasers and Electro-Optics Society, Sydney, NSW, 2005, 422–423
4. Zhuang Y L, Chang W S C, Yu P K L. Peripheral-coupled-waveguide MQW electroabsorption modulator for near transparency and high spurious free dynamic range RF fiber-optic link. IEEE Photonics Technology Letters, 2004, 16(9): 2033–2035
5. Chiu Y J, Wu T H, Cheng W C, Lin F J, Bowers J E. Enhanced performance in traveling-wave electroabsorption modulators based on undercut etching the active-region. IEEE Photonics Technology Letters, 2005, 17(10): 2065–2067
6. Morrison G B, Raring J W, Wang C S, Skogen E J, Chang Y C, Sysak M, Coldren L A. Electroabsorption modulator performance predicted from band-edge absorption spectra of bulk, quantum-well, and quantum-well-intermixed InGaAsP structures. Solid-State Electronics, 2007, 51(1): 38–47
7. Miyazaki Y, Tada H, Tokizaki S, Takagi K, Hanamaki Y, Aoyagi T, Mitsui Y. dBm average optical output power operation of small-chirp 40-gbps electroabsorption modulator with tensile-strained asymmetric quantum-well absorption layer. IEEE Journal of Quantum Electronics, 2003, 39(8): 1009–1017
8. Shim J, Liu B, Bowers J E. Dependence of transmission curves on input optical power in an electroabsorption modulator. IEEE Journal of Quantum Electronics, 2004, 40(11): 1622–1628
9. Abedi K, Ahmadi V, Darabi E, Moravvej-Farshi M K, Sheikhi M H. Design of a novel periodic asymmetric intra-step-barrier coupled double strained quantum well electroabsorption modulator at 1.55 μm. Solid-State Electronics, 2008, 53(2): 312–322
10. Abedi K, Ahmadi V, Moravvej-Farshi M K. Optical and microwave analysis of mushroom-type waveguides for traveling wave electroabsorption modulators based on asymmetric intra-step-barrier coupled double strained quantum wells by full-vectorial method. Optical and Quantum Electronics, 2009, 41(10): 719–733
11. Abedi K. Improvement of saturation optical intensity in electroabsorption modulators with asymmetric intra-step-barrier coupled double strained quantum wells. The European Physical Journal Applied Physics, 2011, 56(1): 10403
12. Abedi K. Improvement in performance of traveling wave electroabsorption modulator with asymmetric intra-step-barrier coupled double strained quantum wells the active region, segmented transmission-line and mushroom-type waveguide. Optical and Quantum Electronics, 2012, 44(1–2): 55–63
13. Abedi K. The design of electroabsorption modulators with negative chirp and very low insertion loss. Journal of Semiconductors, 2012, 33(6): 064001
14. Abedi K. High-performance traveling-wave electroabsorption modulators utilizing mushroom-type waveguide and periodic transmission line loading. Optoelectronics Letters, 2012, 8(3): 176–178
15. Abedi K, Afrouz H. High performance hybrid silicon evanescent traveling wave electroabsorption modulators. Acta Physica Polonica A, 2013, 123(2): 415–417
16. Abedi K. High-performance optical wavelength-selective switches based on double ring resonators. Optoelectronics Letters, 2013, 9 (3): 185–188
17. Abedi K. Design and modeling of traveling wave electrode on electroabsorption modulator based on asymmetric intra-step-barrier coupled double strained quantum wells active layer. International Journal of Advances in Engineering & Technology,, 2011, 1(4): 388–394
18. Abedi K. Effects of geometrical structure on microwave and optical properties of traveling wave electroabsorption modulators based on asymmetric coupled strained quantum wells active layer. International Journal of Engineering Science and Technology, 2011, 3(8): 6684–6691
19. Abedi K. An investigation of strain effect on saturation optical intensity in electroabsorption modulators based on asymmetric quantum wells. Canadian Journal on Electrical and Electronics Engineering, 2011, 2(6): 209–215
20. Jirauschek C. Accuracy of transfer matrix approaches for solving the effective mass schrödinger equation. IEEE Journal of Quantum

Electronics, 2009, 45(9): 1059 –1067

21. Pires M P, Souza P L D, Yavich B, Pereira R G, Carvalho W. On the optimization of InGaAs–InAlAs quantum-well structures for electroabsorption modulators. Journal of Lightwave Technology, 2000, 18(4): 598–603
22. Ohtoshi T. Numerical analysis of α parameters and extinction ratios in InGaAsP-InP pptical modulators. IEEE Journal of Selected Topics in Quantum Electronics, 2003, 9(3): 755–762
23. Hou L P, Wang W, Zhu H L. Optimization design of an electroabsorption modulator integrated with spot-size converter. Optoelectronics Letters, 2005, 1(2): 83–87
24. Shin D S. Waveguiding effect in electroabsorption modulators: passivation layers and their impact on extinction ratios. ETRI Journal, 2005, 27(1): 95–101